Thin Solid Films 519 (2011) 3509–3515

Contents lists available at ScienceDirect

Thin Solid Films

journal homepage: www.elsevier.com/locate/tsf

Control of the optical properties of silicon and chromium mixed oxides deposited by reactive magnetron sputtering

L. Vergara [a,*], R. Escobar Galindo [a,b], R. Martínez [c], O. Sánchez [a], C. Palacio [d], J.M. Albella [a]

[a] Instituto de Ciencia de Materiales de Madrid, Consejo Superior de Investigaciones Científicas, Cantoblanco, 28049 Madrid, Spain
[b] Centro de Microanálisis de Materiales, Universidad Autónoma de Madrid, Cantoblanco, 28049 Madrid, Spain
[c] AIN, Centro de Ingeniería Avanzada de Superficies, 31191 Cordovilla, Pamplona, Spain
[d] Departamento de Física Aplicada, Universidad Autónoma de Madrid, Cantoblanco, 28049 Madrid, Spain

ARTICLE INFO

Article history:
Received 5 March 2010
Received in revised form 27 December 2010
Accepted 5 January 2011
Available online 22 January 2011

Keywords:
Reactive magnetron sputtering
Mixed oxides
Optical properties

ABSTRACT

The development of mixed-oxide thin films allows obtaining materials with better properties than those of the different binary oxides, which makes them suitable for a great number of applications in different fields, such as tribology, optics or microelectronics. In this paper we investigate the deposition of mixed chromium and silicon oxides deposited by reactive magnetron sputtering with a view to use them as optical coatings with an adjustable refractive index. These films have been characterized by means of Rutherford backscattering spectrometry, Auger electron spectroscopy, X-ray diffraction, scanning electron microscopy, Fourier-transform infrared spectroscopy and spectroscopic ellipsometry so as to determine how the deposition conditions influence the characteristics of the material. We have found that the deposition parameter whose influence determines the properties of the films to a greater extent is the amount of oxygen in the reactive sputtering gas.

© 2011 Elsevier B.V. All rights reserved.

1. Introduction

In the last decades, a significant progress in technological areas related to the use of thin films as hard coatings [1–4], combustible cells [5–8], antireflecting cells [9,10] or microelectronics [11–13], has taken place. This is due, to a large extent, to the great development of the techniques involved both in the preparation and in the characterization of the different types of thin films.

The increasing need for a better performance in these fields has led to the development of mixed thin films so as to improve their characteristics as against those of the corresponding different binary compounds. At present, for example, ternary nitrides are prepared to synthesize superhard coatings consisting of nanocrystals of a hard material embedded into an amorphous nitride matrix [14–17]. Another example of this trend is the use of mixed oxides for a great variety of applications, with a view to improving the behaviour of the isolated simple oxides. These applications include active layers in photocatalysis [18–20], gate insulators in complementary metal-oxide-semiconductor structures [21–23], optical coatings with adjustable refractive index [24–26], materials with high dielectric constant [27,28], etc. The applications of each material are given by the choice of oxides, their deposition method, electronic structure and kind of chemical bonds, crystalline structure and morphology, thermal stability, amount of impurities, etc. Therefore, a thorough knowledge about all the processes involved in the synthesis of the thin films is required in order to control their properties and, thus, the applications for which they are suitable.

Several chemical vapour deposition (CVD) techniques have been reported as appropriate for the deposition of mixed oxide thin films, especially PECVD (Plasma Enhanced CVD) [29,30] and IBICVD (Ion Beam Induced CVD) [31,32]. However, these techniques pose some problems associated to the use of metalorganic precursors, like the incorporation of chlorine, hydrogen or carboxyl groups to the films [32,33]. For this reason, an alternative deposition technique must be developed. Reactive sputtering is a promising candidate, since it is a well-known and much studied technique in the field of thin films for a great variety of applications. Moreover, it has the advantage of allowing the growth of compact films with an easily-controllable composition, which is of the utmost importance if they are intended for optical applications in which the refractive index may be controlled by varying the composition of the films or their porosity.

Chromium oxide (Cr_2O_3) is the hardest oxide that also exhibits low friction coefficient, high wear and corrosion resistance, chemical inertness and good optical characteristics [34–36]. This makes it an optimum material to be included in mixed thin films used, for example, for tribological applications (protective coatings), optical applications (solar absorber materials), microelectronic applications, etc. [37–40]. Apart from this, both planar electronics processing and the modern integrated-circuit industry have been made possible by the unique properties of silicon oxide (SiO_2), the only native oxide of a common semiconductor which is stable in water and at elevated

* Corresponding author.
E-mail address: vergara@icmm.csic.es (L. Vergara).

0040-6090/$ – see front matter © 2011 Elsevier B.V. All rights reserved.
doi:10.1016/j.tsf.2011.01.103

temperatures, an excellent electrical insulator, a mask to common diffusing species, and capable of forming a nearly perfect electrical interface with its substrate [41,42].

The purpose of the present work is to investigate mixed Cr_2O_3/SiO_2 thin films so as to determine whether they can be used as optical coatings with a refractive index (n) that can be tailored in a wide range (that is, between 1.45 and 2.75, since these are the values of n for bulk SiO_2 and Cr_2O_3, respectively [36,43]). With this aim in mind, we have investigated the way in which the properties of these mixed-oxide thin films deposited by reactive sputtering are influenced by the deposition parameters.

2. Experimental details

Mixed silicon and chromium oxide films were deposited on (100) silicon substrates by DC magnetron sputtering of a chromium/silicon (80/20 at.%) compound target in a high-purity (99.999%) argon and oxygen atmosphere. The sputtering chamber was pumped down to a base pressure below 8.6×10^{-4} Pa before letting in the gas mixture. Prior to the deposition of each sample, while covering the substrates with a shutter, the target was sputtered with argon for 10 min in order to clean its surface, and then oxygen was let inside the chamber. Only after the target was poisoned the shutter was removed. The substrate holder, placed at a distance of 12 cm from the target, was electrically isolated, with no bias voltage applied externally. Likewise, no intentional heating of the substrates was performed during deposition. The sputtering parameters that were varied in order to determine their influence on the properties of the material were the relative amount of oxygen in the reactive gas (between 1.5% and 5.9%) for a working pressure of around 1 Pa and the DC power (between 80 W and 120 W). The sputtering time was always 60 min, leading to different film thicknesses (from 0.21 to 1.32 μm) that were determined with a Veeco Dektak 150 stylus surface profiler by measuring the height of a step left by a mechanical mask and by cross-sectional scanning electron microscopy (SEM) observation.

Rutherford Backscattering Spectrometry (RBS) experiments were performed with the 5 MV HVEE Tandetron accelerator of the Centro de Microanálisis de Materiales (CMAM) of the Universidad Autónoma de Madrid (UAM). Spectra were collected using a 3.035 MeV He^+ beam, in order to improve the sensitivity to oxygen at the non-Rutherford cross section resonance $^{16}O(\alpha,\alpha)^{16}O$. Data were acquired simultaneously with two silicon surface barrier detectors located at scattering angles of 170° with an energy resolution of 16 keV and an ion dose of 10 μC per detector. The experimental spectra were fitted using the program RBX [44]. Auger electron spectroscopy (AES) measurements were carried out in an ultra-high vacuum chamber at a base pressure below 10^{-7} Pa using a cylindrical mirror analyzer (CMA) provided by VARIAN, with a nominal resolution of 0.25%. The angle between the CMA axis and the normal to the surface of the sample was 30°. The spectra were recorded in the N′(E) mode using a modulation voltage of 2 V_{pp}. In order to avoid electron beam effects on the analyzed layer, we used a constant primary electron beam current density of 10^{-3} A/cm^2 at 3 keV. Sputter depth profiling was carried out using an Ar^+ ion current density of about 0.17 A/m^2 at 3 keV. The angle between the ion gun and the normal to the surface of the sample was approximately 47°. The ion beam was rastered over an area of 10×10 mm^2. Instrumental effects during sputter depth profiling were avoided by aligning carefully the electron and ion beams by means of a Faraday cup. The peak-to-peak heights of the Si LVV, C KLL, Cr LMM and O KLL signals were recorded as a function of time. The crystallinity of the films was assessed by grazing incidence X-ray diffraction (XRD) carried out at an angle of 1.5° with a Panalytical X'Pert PRO theta/theta diffractometer, using the Cu $K\alpha_{1,2}$ doublet with a graphite monocromator to leave out the Kβ line. SEM characterization was carried out by means of two field emission scanning electron microscopes (FE-SEM), an FEI Nova NanoSEM 230 for the top-view images and an INCAx-sight FE-SEM with a resolution of 136 eV when operating at 5.9 keV for the cross-sectional qualitative element mapping and images. Fourier-transform infrared (FT-IR) transmittance spectra were obtained with a Bruker IFS60v spectrometer using non-polarized light between 560 cm^{-1} and 7000 cm^{-1} with a mercury–cadmium–telluride detector. Spectroscopic ellipsometry was employed to determine the refractive index and the absorption coefficient of the films in the visible range (from 400 nm to 900 nm); measurements were performed with an M-2000U ellipsometer working in the range of 250–1600 nm with an incidence angle of 70°.

3. Results and discussion

Table 1 shows the variable deposition parameters for the four representative samples we have analysed in this work.

As was expected, the thickness of the films – the average of the values obtained by profilometry and SEM – depends on their deposition conditions. Provided the other deposition parameters remain constant, the higher the DC power generating the plasma, the higher the thickness of the films. Additionally, for the same power, the thickness of the films depends on the composition of the gas, and is higher when the content of oxygen is smaller. The extraction efficiency of argon ions is higher than that of oxygen ions, owing to the difference in their masses [45,46]. Therefore, a reduction in the oxygen content, for the same working pressure, gives rise to an increase in the number of argon ions reaching the target and, thus, in the thickness of the films.

RBS measurements (see Fig. 1) allowed us to determine the density and composition of the films, by using the thickness of the layers included in Table 1. These results are summarized in Table 2, and show that samples A and B are homogeneous in composition and have well-defined interfaces, as they can be properly fitted by using a single layer structure. On the contrary, the interfaces of samples C and D are not so clearly defined, with some diffusion taking place. In particular, two layers are required to fit the simulation to the experimental data in the case of sample C, since for this sample the diffusion reaches more than half the thickness of the overall film; the thickness of these two layers are 400 nm for the top layer and 560 mn for the bottom layer. Finally, the presence of a broad interface profile in sample D is evident from the disagreement between the RBS simulation (which has been carried out using a sharp interface) and the experimental data. Regarding the composition of the films, they can also be divided into two groups, which coincide with those defined by the structural differences mentioned above. On the one hand, the content of chromium in samples A and B is lower (around 10 at.%) than that of silicon (around 20 at.%). Both samples have a high amount of oxygen (over 60 at.%), which results in a low ratio of metal (chromium plus silicon) to oxygen contents, between 0.4 and 0.5 for these two samples. The densities of these layers, as derived from the RBS measurements, are approximately 2 g/cm^3, that is, lower than that of stoichiometric SiO_2 (2.5 g/cm^3); therefore, we can describe these two samples as $Si(Cr)O_x$, with $x>2$ (that is, sub-stoichiometric silicon dioxide with chromium partly replacing silicon). In sample C, the silicon content is very low (between 5 and 6 at.%) and that of chromium is high (over 30 at.%), while the amount of oxygen is slightly lower than for samples A and B (about 60 at.%). There is an small increase in the chromium content (from 31 to 34 at.%), and a subsequent decrease in that of oxygen (from 59 to

Table 1
Deposition conditions for samples A–D.

Sample	% O_2	Power (W)	Thickness (μm)	Deposition rate (nm/min)
A	5.9	80	0.21 ± 0.04	3.5 ± 0.7
B	5.9	120	0.35 ± 0.10	5.9 ± 1.8
C	1.5	80	0.96 ± 0.12	16.0 ± 2.1
D	1.5	120	1.32 ± 0.04	22.0 ± 0.7

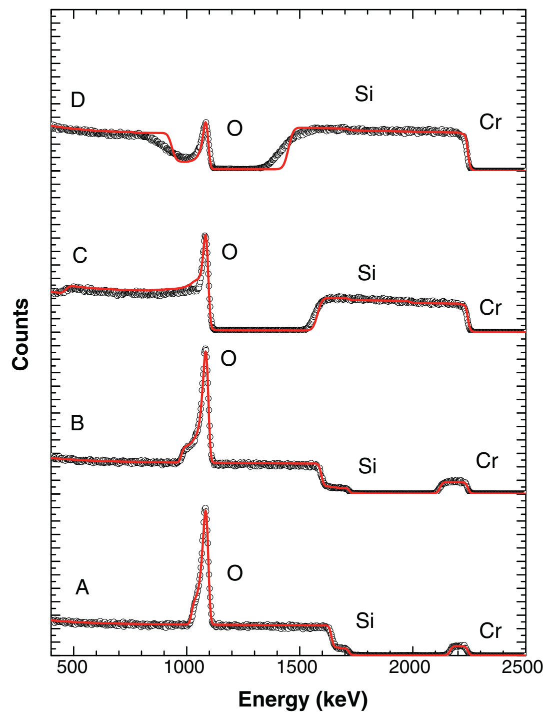

Fig. 1. RBS spectra of samples A (bottom) to D (top): experimental data (open circles) and simulation (solid line).

54 at.%) when comparing the top and the bottom layers. These changes in the composition of the films are related to an increase in the density from 4.5 to 5.1 g/cm^3. At the same time, the ratio of metal to oxygen also rises from 0.6 to 0.7. In stoichiometric Cr_2O_3 oxides, the ratio of chromium to oxygen is 0.67, with a density of 5.2 g/cm^3. Thus, sample C can be described as dichromium trioxide with silicon inclusions ($Cr(Si)_2O_3$). Finally, although the silicon content of sample D remains similar to that of sample C (6 at.%), there is a clear increase in that of chromium, as well as a reduction in the oxygen concentration; this results in a ratio of metal to oxygen of 1.5 and a total contribution of the metals of 30%. As will be proven later, this is related to the presence of metallic chromium in the layer, so this sample can be described as $Cr_{met}+Cr(Si)_2O_3$. The presence of such a high amount of metallic chromium is due to the fact that sample D was deposited at a high DC power (120 W), which increased the rate of extraction of material from the chromium-rich target. At the same time, the low percentage of oxygen in the plasma was not enough to react with all the chromium sputtered from the target, so it reached the substrate in metallic form; this effect was enhanced by the higher extraction efficiency of an atmosphere rich in argon. It is also worth noting that all the samples contain a certain amount of carbon, always on their surface, owing to contamination of the samples when exposed to room atmosphere after deposition.

AES has allowed us to obtain complementary chemical information about the samples, and has corroborated the presence of a high carbon content in sample D. Fig. 2(a) shows the low-energy AES spectrum involving the Cr MVV and Si LVV transitions for this sample after a two-minute bombardment with Ar^+, while Fig. 2(b) shows the C KLL transition, as well as the overlapping between the Cr LMM and O KLL transitions for the same sample and the same bombardment conditions. It follows from Fig. 2(a) that the bombarded surface is characterized by four peaks at 27.7, 33, 42 and 77 eV. Those located at 33 and 42 eV are assigned to the Cr MVV transition in the oxide and to autoionization, respectively, and are therefore consistent with the presence of Cr_2O_3 in the sample [47]. A peak at 76 eV is expected for SiO_2 [48]; the observed shift for this peak and the peak at 27.7 eV point to the formation of a Cr–Si mixed oxide. In addition, the average concentration of chromium, oxygen, silicon and carbon, derived from the AES depth profile using sensitivity factors for each element, is 40%, 36%, 13% and 9%, respectively. There is a fair agreement between these results and those obtained by RBS for chromium and oxygen, with a slight deviation in the case of silicon and carbon. Although such differences could be attributed to preferential sputtering effects owing to the bombardment with Ar^+, it should be pointed out that these are very difficult to explain for this complicated quaternary system, so further work in this direction is required.

These samples were also analysed by XRD in order to determine their crystallinity; the diffraction patterns are shown in Fig. 3. As can be seen, samples A, B and C are virtually amorphous, with traces of very broad peaks centred at approximately $2\theta=23°$ for samples A and B (typically attributed to amorphous SiO_2 [49]), and at 35° for sample C (corresponding to a chromium-rich oxide [50]). In the case of the diffraction pattern of sample D, there is a distinctive peak centred on 44.4° corresponding to metallic chromium [36], which corroborates our explanatory theory about the high chromium content in this sample detected by RBS, discussed above.

Table 2
Density and composition of samples A–D, obtained by RBS. Two different layers (top and bottom) have been necessary to adjust sample C, so data are given for both.

Sample	Density (g/cm^3)	Cr (at.%)	Si (at.%)	O (at.%)	C (at.%)	(Cr + Si)/O
A	2.1	9	17	64	10	0.41
B	2.0	12	17	62	10	0.47
C_{top}	4.2	31	5	59	5	0.61
C_{bottom}	4.5	34	6	55	5	0.73
D	4.0	45	6	34	15	1.5

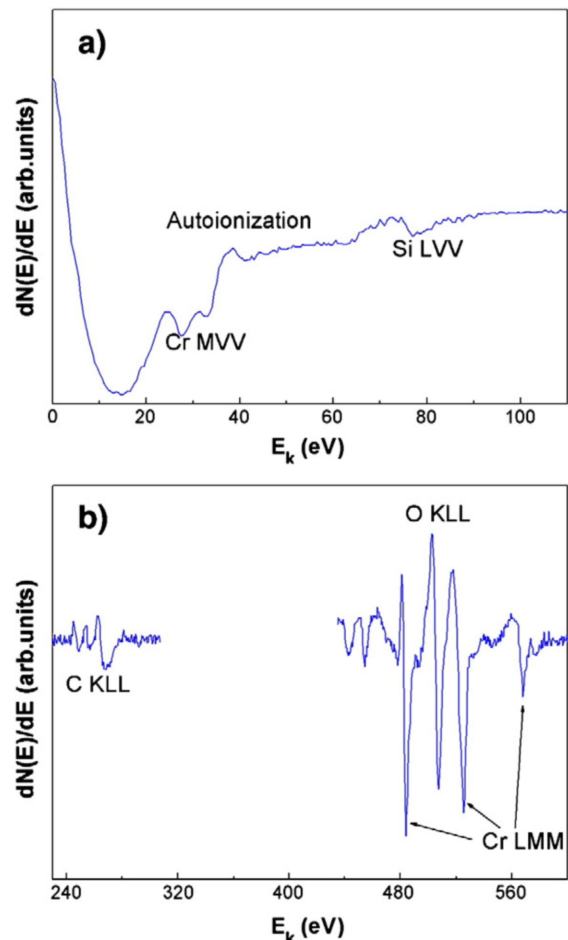

Fig. 2. AES spectra of sample D after a two-minute bombardment with argon ions.

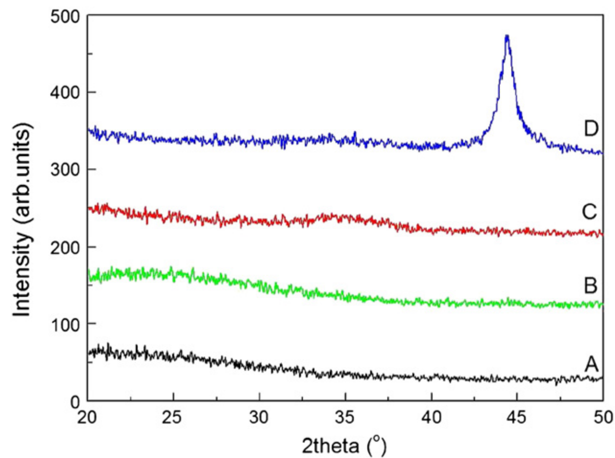

Fig. 3. XRD patterns of samples A (bottom) to D (top).

Fig. 4 shows top-view SEM images of the four samples under study. As can be seen, the aspect of their surface evolves from the smoother surface of samples A, B and C to the rougher one of sample D.

In order to delve into the study of the structure of the four films, we obtained cross-sectional SEM images, which are shown in Fig. 5. Once again, there is a clear distinction between samples deposited at high (A and B) and low (C and D) oxygen flux. While the former present a dense featureless morphology, sample C presents an incipient columnar growth, which becomes clearly evident in sample D. According to XRD measurements, metallic chromium must be responsible for this remarkable columnar structure of sample D.

We also obtained mapping images of these cross-sectional images for the four samples (presented in Fig. 6), in order to determine the distribution of each of the chemical elements within the films. These results clearly point in the same direction as the RBS measurements, inasmuch as there is an obvious distinction between two groups of samples, A and B, on the one hand, and C and D, on the other. In accordance with the RBS data in Table 2, the amount of chromium (green dots) in samples C and D is much higher than in samples A and B, in which the predominant metallic element is silicon (red dots). The image of sample C evidences the double-layer structure already suggested by the RBS measurements: in particular, and in agreement with them, it can be observed that the oxygen content (blue dots) in the top layer is higher than in the bottom one. In sample D, chromium seems not to be combined with oxygen to the same extent as in the rest of samples, which would account for its presence in metallic form. This is also supported by the evolution of the Cr MVV AES transition during depth profiling (not shown), in which a new peak at 35 eV, indicative of metallic character, appears in addition to the peak at 33 eV (associated, as we mentioned previously, to chromium oxide) as the profiling approaches the interface with the substrate. It can also be observed that the interface between the film and the substrate is much less defined in samples C and D than in samples A and B, which had already been proved by the RBS measurements.

FT-IR measurements were carried out in order to determine the chemical bonds present in the amorphous deposited coatings. Fig. 7 shows the spectra of the four samples described in Table 1. Although measurements have been carried out up to 7000 cm^{-1}, Fig. 7 is restricted only to the window between 560 cm^{-1} and 2000 cm^{-1}, so as to display the area of interest in a greater detail. The only feature in the spectra outside the shown area is a broad band at approximately 3200 cm^{-1} in samples A, B and C, which we have attributed to structural hydroxyl groups [51,52]. The bands between 1400 cm^{-1} and 1600 cm^{-1} also correspond to OH species [52], while those appearing at 610 cm^{-1} are a consequence of the scattering of the light

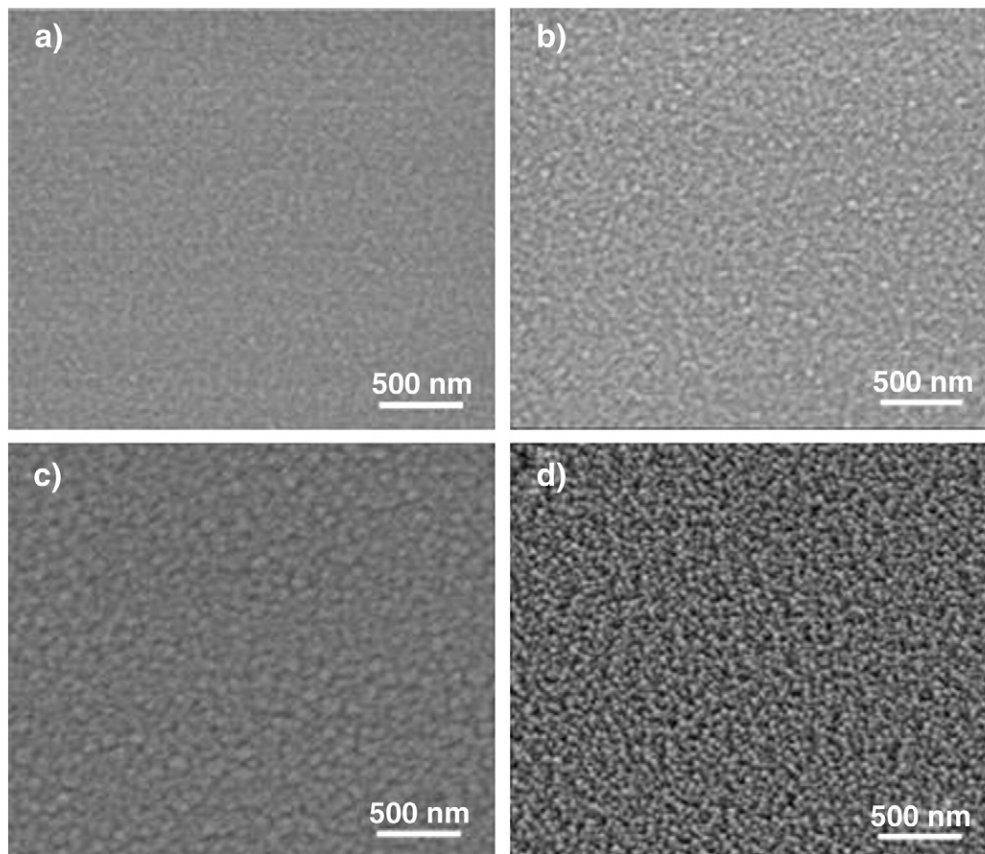

Fig. 4. Top-view SEM photographs of samples a, b, c and d (magnification of ×100 k).

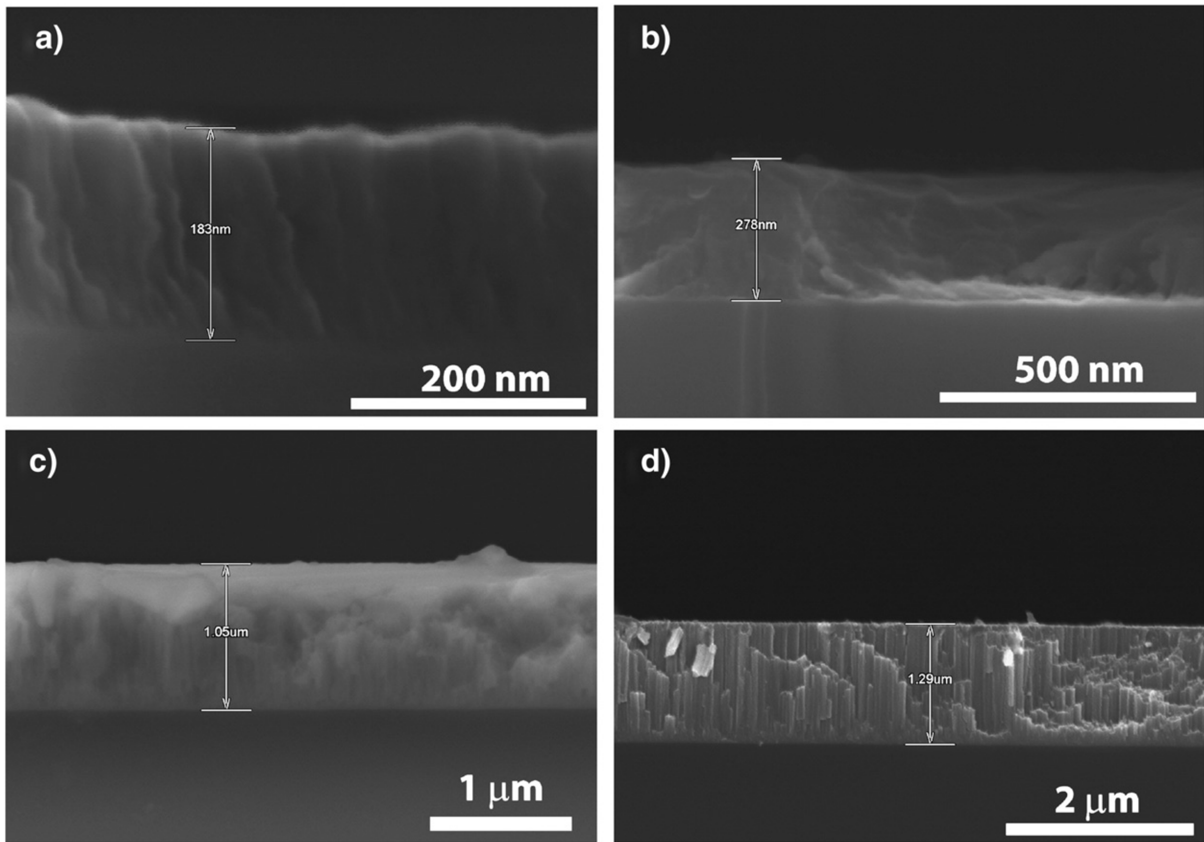

Fig. 5. Cross-sectional SEM photographs of samples a, b, c and d. Magnifications of ×250 k, ×110 k, ×30 k and ×20 k, respectively.

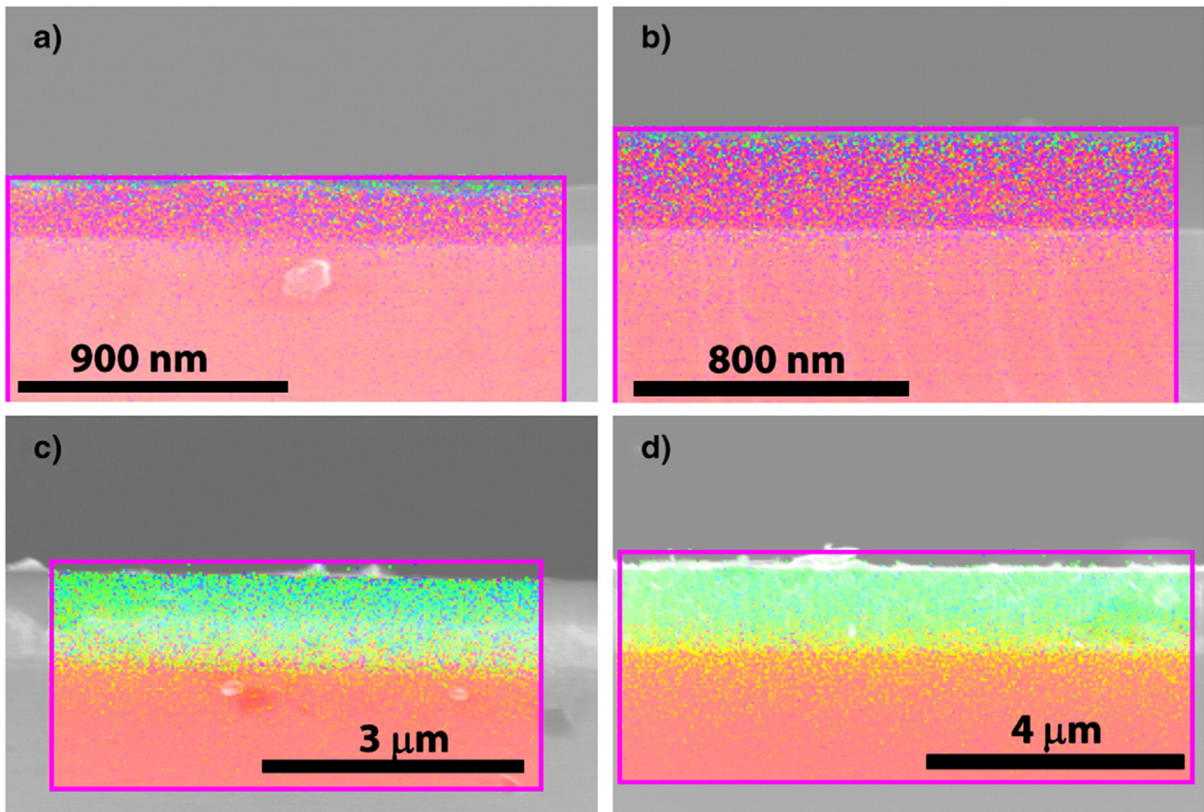

Fig. 6. Transversal sections of samples a to d: compound images from the separate mapping images of silicon (red), chromium (green) and oxygen (blue).

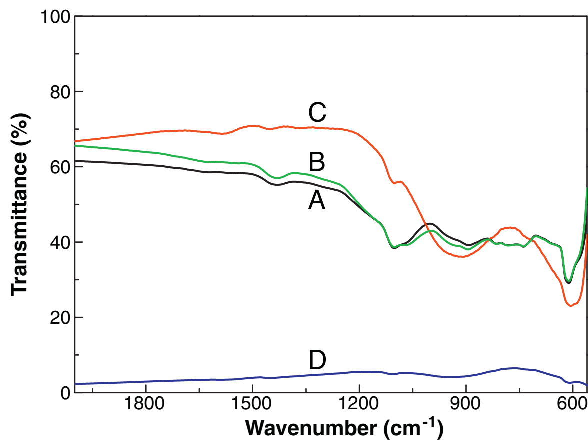

Fig. 7. FT-IR transmittance spectra of samples A to D.

by electric dipoles that result from the oxidation of the surface of the silicon substrate [53]. The most striking feature of the spectra in Fig. 7 is the comparatively low transmittance of sample D as compared to that of the other three samples. This can be easily explained both by its higher thickness and by the presence of metallic material reflecting part of the incident signal. Once again, Fig. 7 provides evidence for the existence of two different sets of samples, A and B on the one side, and C and D on the other. The spectra of samples C and D (taking into account the differences owing to the attenuation of the spectra of sample D) show a similar aspect, and so do the spectra of samples A and B, to the extent of overlapping almost completely in the low wavenumber zone. Absorption bands around 1100 cm^{-1} are known to be related to the infrared active vibrations of the Si–O–Si bonds, present in all SiO_x films, whose frequency of vibration depends on the environment of the silicon atoms. In particular, it is the frequency of the Si–O–Si asymmetric stretching mode for SiO_2 which appears about 1100 cm^{-1} [54,55]. All the spectra in Fig. 7 present these weak bands around 1100 cm^{-1}, which shows that there is a low amount of Si–O bonds in all the samples, in accordance with their low silicon contents detected by RBS (see Table 2). The large, broad band at 920 cm^{-1} for sample C (traces of which can also be spotted in the spectra of sample D), less intense for samples A and B, probably characterizes oxygen species of the Cr–O–Cr type [56]. Our RBS results also predicted this behaviour, by determining that the amount of chromium in samples C and D was much higher than in samples A and B, leading to a higher number of Cr–O bonds.

Ellipsometry measurements in the visible range, shown in Fig. 8, have allowed us to determine both the refractive index (n) and the extinction coefficients (k) of the films. The oxide layers were fitted using Cauchy's Eq. (1), which describes the dispersion of the refractive index of the film as a slowly-varying function of wavelength (with an exponential absorption tail [57]. The results of the fitting are summarized in Table 3.

$$n(\lambda) = B_0 + \frac{B_1}{\lambda^2} + \frac{B_2}{\lambda^4}$$
$$\kappa(\lambda) = \kappa_{amp} e^{-a\lambda} \qquad (1)$$

The model includes a 5 nm-thick layer of native oxide on top of the silicon substrate. It is worth noting that the only modelling that required the inclusion of a significant roughness (of approximately 20 nm) was that of sample D, in accordance with the SEM observations of Fig. 4. The ellipsometry measurements yielded refractive index values of 1.60, 1.61 and 2.75 at 600 nm for samples A, B and D, respectively. However, the behaviour of sample C was reproduced better when using two different oxide layers than when using only one, which agrees with the RBS measurements (Fig. 1) and the cross-sectional SEM mapping (Fig. 6). The bottom layer has a thickness of 560 nm and a refractive index of 2.30 at 600 nm, while the top layer was forced to have a thickness of 400 nm, and has a higher refractive index of 2.57 at 600 nm. Additionally, the values of the absorption coefficient at 600 nm of the four samples, determined from the measurements shown in Fig. 8(b), are of 0.04 (samples A and B), 0.15 (sample C, bottom layer), 0.18 (sample C, top layer) and 1.30 (sample D). The refractive index and extinction coefficient of SiO_2 are 1.45 and <0.1 at 600 nm, respectively [58]; they are commonly assumed to be of 2.5 and 0.1, respectively, for Cr_2O_3, although it is known that they can vary depending on the oxygen content in the film. Our values are within the reported ranges, as the refractive index and extinction coefficient of chromium oxide change from 2.3 to 2.7 and from 0.07 to 0.22, respectively, when increasing the amount of oxygen in the deposition chamber during deposition [59]. Finally, the values of n and k at 600 nm for metallic chromium are 3.19 and 3.30, respectively [58]. These values allow us to conclude that, as was the case with all the previous results presented in this work, the four samples under study can be distributed into two separate groups. The optical properties of samples A and B are very similar to those of SiO_2, although with slightly higher values of both n and k (which can be attributed to the low amount of chromium present in the films). We have already described sample C as dichromium trioxide with silicon inclusions, and the ellipsometry results do support this assumption. Finally, the behaviour of sample D, with higher n and k values, can be perfectly explained by the presence of metallic chromium in the structure of the films.

It should be noted that all the data that we have presented in this work are in remarkably good agreement as to the different behaviour of samples A and B as opposed to that of samples C and D, which allows determining in an unequivocal way that the amount of oxygen in the plasma represents the main factor influencing the properties of the films. As far as the structural characteristics of the samples are

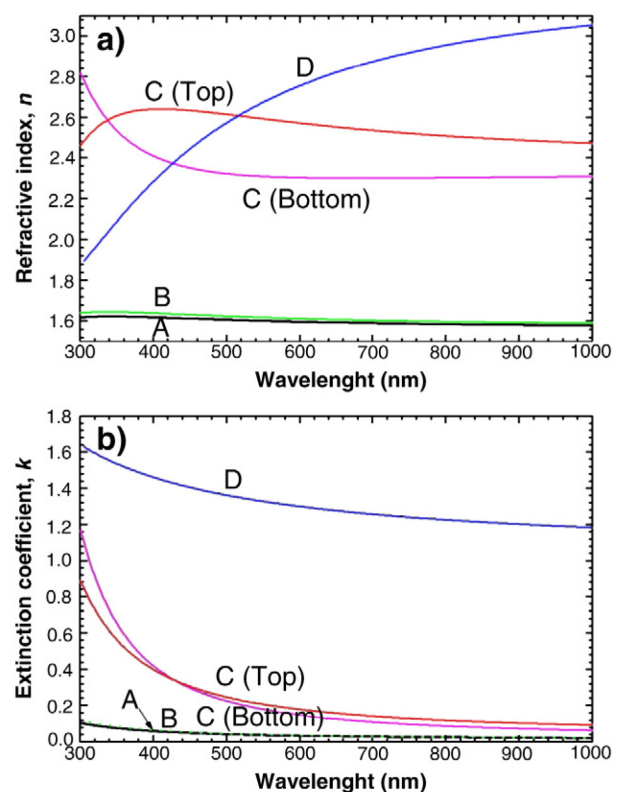

Fig. 8. Ellipsometry measurements of samples A to D: (a) Refractive index and (b) Extinction coefficient, as a function of the wavelength. Sample C has been simulated by means of two different layers.

Table 3
Values of the adjustable parameters used to fit the experimental refractive index and absorption coefficient of samples A to D using Eq. (1). Two different layers (top and bottom) have been necessary to adjust sample C, so data are given for both.

Sample	B_0	B_1 (nm^2)	B_2 (nm^4)	k_{amp}	α (nm^{-1})
A	1.573 ± 0.002	0.0340 ± 0.001	−0.0034 ± 0.0001	0.068 ± 0.001	1.432 ± 0.064
B	1.583 ± 0.002	0.0186 ± 0.001	−0.0013 ± 0.0002	0.072 ± 0.001	0.737 ± 0.060
C_{top}	2.348 ± 0.001	0.0816 ± 0.001	−0.0069 ± 0.0001	0.402 ± 0.002	0.776 ± 0.005
C_{bottom}	2.331 ± 0.001	−0.0280 ± 0.001	0.0065 ± 0.0003	0.421 ± 0.004	1.001 ± 0.005
D	3.240 ± 0.003	−0.1918 ± 0.002	0.0062 ± 0.0004	1.462 ± 0.003	0.113 ± 0.001

concerned, both RBS and SEM measurements show that the interface between the substrate and the oxide layer in samples A and B, deposited with a higher oxygen percentage than samples C and D, is more clearly defined. Samples A and B present no clear morphology, while samples C and D have a columnar structure, more prominent in the case of sample D, probably owing to the presence of metallic chromium (evidenced also by XRD measurements). Additionally, both of these techniques point to the existence of two layers with different characteristics within sample C owing to the marked diffusion that takes place in this sample. From a chemical point of view, all the characterization techniques we have employed (RBS, AES, SEM mapping images and FT-IR) prove that the chromium content of those samples (A and B) deposited using a plasma rich in oxygen is much lower than in the case of the samples deposited with a lower amount of oxygen in the plasma (C and D). Ellipsometry corroborates the double-layer structure of sample C and, besides, in accordance with the different distribution of chromium and silicon in the two groups of samples made evident by the chemical characterization techniques, shows that the optical properties (refractive index and extinction coefficient) of samples A and B are similar to those of SiO_2 (with a higher refractive index owing to the partial replacement of silicon with chromium), while those of samples C and D are closer to those of Cr_2O_3 and $Cr_2O_3 + Cr$, respectively.

4. Conclusions

Mixed silicon and chromium oxide films were deposited by reactive DC magnetron sputtering varying the applied power and percentage of oxygen in the gas during deposition, so as to investigate the influence of these parameters on the properties of the films. This work presents an analysis of four representative samples that were analysed by means of RBS, AES; XRD, SEM, FT-IR and ellipsometry. All these techniques point towards the distribution of the samples into two groups, depending on the oxygen content, whose influence predominates over that of the applied power. In this way we are able to vary the refractive index of the mixed oxides in a controlled way between those of each of their constituent single oxides, which makes our films suitable for a wide range of applications.

Acknowledgments

This work has been supported by the Ministerio de Ciencia e Innovación of Spain through the Consolider-Ingenio 2010 programme (CSD2008-00023) and through projects MAT2008-06618-C02-02/MAT and RyC2007-0026.

References

[1] S. Labdi, P. Houdy, P. Psyllaki, M. Jeandin, Thin Solid Films 275 (1996) 213.
[2] I.Y. Konyashin, M.B. Guseva, Diam. Relat. Mater. 5 (1996) 575.
[3] T. Kohara, H. Tamagaki, Y. Ikari, H. Fujii, Surf. Coat. Technol. 185 (2004) 166.
[4] Y. Zhang, Y.T. Cheng, D.S. Grummon, Mater. Sci. Eng. A 438–440 (2006) 710.
[5] S.A. Barnett, Energy 15 (1) (1990) 1.
[6] L.G. Coccia, G.C. Tyrrell, J.A. Kilner, D. Waller, R.J. Chater, I.W. Boyd, Appl. Surf. Sci. 96–98 (1996) 795.
[7] P. Bocchetta, G. Chiavarotti, R. Masi, C. Sunseri, F. Di Quarto, Electrochem. Commun. 6 (2004) 923.
[8] Z. Wang, K. Sun, S. Shen, N. Zhang, J. Qiao, P. Xu, J. Membrane. Sci. 320 (2008) 500.
[9] M. Chigane, M. Izaki, Y. Hatanaka, T. Shinagawa, M. Ishikawa, Thin Solid Films 515 (2006) 2513.
[10] X. Wu, W. Zhang, L. Yan, R. Luo, Thin Solid Films 516 (2008) 3189.
[11] J.C. Anderson, Thin Solid Films 12 (1972) 1.
[12] V.I. Petrovsky, A.S. Sigov, Microelectron. Eng. 29 (1995) 11.
[13] M. Leskelä, K. Kukli, M. Ritala, J. Alloy Compd 418 (2006) 27.
[14] S. Vepřek, P. Nesládek, A. Niederhofer, F. Glatz, Nanostruct. Mater. 10 (1998) 679.
[15] P. Nesládek, S. Vepřek, Phys. Status Solidi A 177 (2000) 53.
[16] A. Bendavid, P.J. Martin, E.W. Preston, J. Cairney, Z.H. Xie, M. Hoffman, Surf. Coat. Technol. 201 (2006) 4139.
[17] L. Vergara, O. Sánchez, J.M. Albella, Vacuum 83 (2009) 1233.
[18] Y. Guo, D. Li, C. Hu, E. Wang, Y. Zou, H. Ding, S. Feng, Microporous Mesoporous Mater. 56 (2002) 153.
[19] C. Wang, B.Q. Xu, X. Wang, J. Zhao, J. Solid State Chem. 178 (2005) 3500.
[20] A. Kubacka, M. Fernández-García, G. Colón, J. Catal. 254 (2008) 272.
[21] J. Kwo, M. Hong, B. Busch, D.A. Muller, Y.J. Chabal, A.R. Kortan, J.P. Mannaerts, B. Yang, P. Ye, H. Gossmann, A.M. Sergent, K.K. Ng, J. Bude, W.H. Schulte, E. Garfunkel, T. Gustaffson, J. Cryst. Growth 251 (2003) 645.
[22] L. Houssiau, R.G. Vitchev, T. Conard, W. Vandervorst, H. Bender, Appl. Surf. Sci. 231–232 (2004) 585.
[23] A.A. Dakhel, Microelectron. Reliab. 48 (2008) 395.
[24] F. Varsano, F. Decker, E. Masetti, F. Cardenilli, A. Licciulli, Electrochim. Acta 44 (1999) 3149.
[25] F. Gracia, F. Yubero, J.P. Holgado, J.P. Espinos, A.R. González-Elipe, T. Girardeau, Thin Solid Films 500 (2006) 19.
[26] S. Lisinski, J. Krause, D. Schaniel, L. Ratke, T. Woike, Scr. Mater. 58 (2008) 553.
[27] M. Bizarro, J.C. Alonso, A. Ortiz, Mater. Sci. Semicond. Proc. 9 (2006) 1090.
[28] M. Veith, S. Ren, M. Wittmar, H. Bolz, J. Solid State Chem. 182 (2009) 2930.
[29] Z. Cao, R. Owen, Thin Solid Films 271 (2995) 69.
[30] A. Dittmar, M. Schneider, J. Radnik, E. Kondratenko, D. Herein, Prog. Solid State Chem. 35 (2007) 249.
[31] A. Stabel, A. Caballero, J.P. Espinos, F. Yubero, A. Justo, A.R. González-Elipe, Surf. Coat. Technol. 100–101 (1998) 142.
[32] F.J. Ferrer, F. Frutos, J. García-López, A.R. González-Elipe, F. Yubero, Thin Solid Films 516 (2007) 481.
[33] F. Gracia, J.P. Holgado, L. Contreras, T. Girardeau, A.R. González-Elipe, Thin Solid Films 429 (2003) 84.
[34] V.M. Bermudez, W.J. DeSisto, J. Vac. Sci. Technol. A 19 (2) (2001) 576.
[35] E. Sourty, J.L. Sullivan, M.D. Bijker, Tribol. Int. 36 (2003) 389.
[36] P. Hones, M. Diserens, F. Lévy, Surf. Coat. Technol. 120–121 (1999) 277.
[37] V. Zieren, M. De Jongh, A. Broese van Groenou, J.B.A. Van Zon, P. Lasinski, G.S.A.M. Theunissen, IEEE T. Magn. 30 (2) (1994) 340.
[38] M.G. Hutchins, Surf. Technol. 20 (1983) 301.
[39] S. Hong, E. Kim, Z.T. Jiang, B.S. Bae, K. No, W. Shin, S.C. Lim, S.G. Woo, Y.B. Koh, Proc. SPIE 2793 (1996) 134.
[40] S. Hong, E. Kim, D.W. Kim, T.H. Sung, K. No, J. NonCryst. Solids 221 (1997) 245.
[41] E.R. Weber, Appl. Phys. Mater. 30 (1983) 1.
[42] K. Xue, H.P. Ho, J.B. Xu, J. Phys. D Appl. Phys. 40 (2007) 2886.
[43] C. Cobianu, C. Pavelescu, A. Paunescu, J. Mater. Sci. Lett. 4 (1985) 1419.
[44] E. Kótai, Nucl. Instrum. Meth. B 85 (1994) 588.
[45] H. Ohsaki, Y. Tachibana, A. Mitsui, T. Kamiyama, Y. Hayashi, Thin Solid Films 392 (2001) 169.
[46] M. Clement, E. Iborra, J. Sangrador, A. Sanz-Hervás, L. Vergara, M. Aguilar, J. Appl. Phys. 94 (3) (2003) 1495.
[47] C. Palacio, H.J. Mathieu, D. Landolt, Surf. Sci. 182 (1987) 41.
[48] L.E. Davis, N.C. McDonald, P.W. Palmberg, G.E. Riach, R.E. Weber, Handbook of Auger Electron Spectroscopy, Physical Electronics Industries, Eden Prairie, Minnesota, 1972.
[49] X. Zhang, D. Zhang, X. Ni, H. Zheng, Mater. Lett. 61 (1) (2007) 248.
[50] M.F. Al-Kuhaili, S.M.A. Durrani, Opt. Mater. 29 (2007) 709.
[51] R. Hofman, J.G.F. Westheim, I. Pouwel, T. Fransen, P.J. Gellings, Surf. Interface Anal. 24 (1996) 1.
[52] I. Idris, O. Sugiura, Jpn. J. Appl. Phys. 34 (1995) L772.
[53] M. Sasanuma, Y. Takeshita, Jpn. J. Appl. Phys. 34 (1995) 5844.
[54] Q. Hu, H. Suzuki, H. Gao, H. Araki, W. Yang, T. Noda, Chem. Phys. Lett. 378 (2003) 299.
[55] W. Bensch, W. Bergholz, Semicond. Sci. Technol. 5 (1990) 421.
[56] M. Trpkovska, B. Šoptrajanov, L. Pejov, J. Mol. Struct. 654 (2003) 21.
[57] H.G. Tompkins, E.A. Irene, Handbook of Ellipsometry, William Andrew Publishing, Norwich, New York, 2005.
[58] E.D. Palik, Handbook of Optical Constants of Solids, Academic Press, New York, 1998.
[59] H.C. Barshilia, K.S. Rajam, Appl. Surf. Sci. 255 (2008) 2925.